CFD based investigations on hydrodynamics and energy dissipation due to solid motion in liquid fluidised bed

R. Panneerselvam, S. Savithri, G.D. Surender *

Process Engineering and Environmental Technology Division, Regional Research Laboratory, Trivandrum 695 019, India

Abstract

CFD simulations are carried out for the prediction of flow patterns in a liquid–solid fluidised bed using Eulerian–Eulerian framework. The CFD model predictions are compared with the experimental findings reported by Limtrakul et al. [S. Limtrakul, J. Chen, P.A. Ramachandran, M.P. Dudukovic, Solids motion and holdup profiles in liquid fluidised beds, Chem. Eng. Sci. 60 (2005) 1909–1920] and the comparison shows good agreement. The CFD model has been further extended to compute solid mass balance in the core and annular regions for verifying conservation of mass and energy flows due to various dissipation mechanisms. Energy required for solid expansion in liquid fluidised bed is also compared with energy required for solid suspension in an equivalent stirred tank contactor at similar operating conditions. The influence of various interphase drag models proposed by Gidaspow [D. Gidaspow, Multiphase Flow and Fluidisation, 1st ed., Academic Press, San Diego, 1994], Di Felice et al. [R. Di Felice, The voidage functions for fluid–particle interaction system, Int. J. Multiphase Flow 20 (1994) 153–159] and Syamlal and O'Brien [M. Syamlal, T.J. O'Brien, Simulation of granular layer inversion in liquid fluidised beds, Int. J. Multiphase Flow 14 (1988) 473–481] on solid motion in liquid fluidised bed have been investigated. Even though these models predict the flow pattern of solid motion inside the fluidised bed with reasonable accuracy, the model proposed by Gidaspow showed the better quantitative agreement with experimental data. For ensuring accuracy of numerical simulation prediction, comparisons between 2D and 3D simulation, the effect of grid sensitivity, time step sensitivity and effect of inlet feed conditions have been carried out and a comprehensive CFD methodology is proposed to model the hydrodynamics of liquid–solid fluidised bed.

© 2007 Elsevier B.V. All rights reserved.

Keywords: CFD; Hydrodynamics; Liquid fluidised beds; Solid circulation

1. Introduction

Liquid–solid fluidised beds continue to attract increasing attention due to their inherent versatility for several industrial applications in hydrometallurgical, biochemical, environmental and chemical process industries [1]. Due to advantages such as the absence of high shear zones and uniform distribution of solids, liquid–solid fluidised beds provide a viable option to replace mechanically agitated reactors for achieving cost reduction and improvements in product quality. However, due to lack of information on various design and operating aspects of liquid–solid fluidised beds, it is likely that their introduction to large scale applications may not be realized as soon as desirable. Significant contributions have been made by several authors [2,3] to improve the understanding of the hydrodynamics of liquid–solid fluidised beds through experimental and theoretical investigations. In comparison to reactors such as the bubble column, the flow patterns of solid in liquid fluidised beds is not yet well understood in terms of circulation patterns and energy dissipation. Circulation phenomena of solids have been observed to be dominant in liquid fluidised beds due to non-uniform solid holdup profiles and solid velocity profiles. For this reason, computational fluid dynamics (CFD) has been promoted as a useful tool for understanding multiphase reactors [4] for reliable design and scale up.

Hydrodynamics and solids expansion in liquid fluidised beds have been extensively studied by several authors [5–7] and reviewed by Di Felice [8]. Kiared et al. [2] who investigated the flow structure of solids in three dimensional liquid fluidised beds using the radioactive particle tracking technique observed that the flow structure consists of a core and an annulus in which the solids displayed distinct upward and downward movements, respectively. Yang and Renken [9] provided an interpretation of the Richardson–Zaki equation by linking the

---

* Corresponding author. Tel.: +91 471 2490518; +91 471 2491712.
E-mail address: geraldsuren@yahoo.com (G.D. Surender).

Nomenclature

a	parameter in Eq. (36)
A, B	coefficient in the Syamlal and O'Brien model
Ar	Archimedes number
C	solid compaction modulus
C_d	drag coefficient
$C_{\mu b}$	coefficient in particle induced turbulence model
$C_\mu, \sigma_k, \sigma_\varepsilon, C_{\varepsilon 1}, C_{\varepsilon 2}$	coefficient in turbulent parameters
d_p	particle diameter (m)
D	column diameter (m)
D_i	impeller diameter in Eq. (46)
D_c	diameter of core region (m)
E_B	rate of energy dissipation by friction between two phases (W)
E_D	energy dissipation by the liquid phase (W)
E_e	energy dissipation rate due to turbulence in liquid phase (W)
E_f	frictional energy loss of liquid phase (W)
E_i	input energy due to liquid phase (W)
E_k	liquid phase turbulent kinetic energy (W)
E_l	potential energy of liquid leaving the fluidised bed (W)
E_s	solid phase potential energy (W)
E_T	energy transfer from liquid to solid in core region (W)
f	ratio of the falling velocity to the terminal velocity of a single particle
f_c	constant in Eq. (46)
F_{TD}	turbulent dispersion force (N)
F_{Dl}	liquid phase interphase drag force (N)
F_{Ds}	solid phase interphase drag force (N)
g	acceleration gravity (m/s^2)
$G(\varepsilon_s)$	solid elastic modulus
G_0	reference elasticity modulus
H	expanded bed height (m)
k	the turbulence kinetic energy (m^2/s^2)
m, C	constants involved in Eq. (28)
n_c	curvature of the velocity profile in Eq. (29)
n	parameter in Eq. (35)
N	impeller speed (rps)
N_{CS}	critical impeller speed for just suspended solid (rps)
N_p	power number
N_{Re}	Impeller Reynolds number
P	liquid-phase pressure (kg/m s^2)
P_s	solids pressure (kg/m s^2)
r/R	Dimensionless radial position
R	radius of column (m)
R_i	radius of inversion
Re	Reynolds number
Re_p	particle Reynolds number
Re_t	Reynolds number based on particle terminal velocity
T	tank diameter (m)

x	empirical coefficient in the Di Felice model
u_l	liquid phase velocity vector (m/s)
u_s	solid phase velocity vector (m/s)
U	superficial velocity (m/s)
U_{mf}	minimum fluidisation velocity (m/s)
U_t	particle terminal fall velocity (m/s)
v_s	time averaged solid velocity in the core region (m/s)
V_l	superficial liquid velocity (m/s)
V_{in}	inlet superficial liquid velocity (m/s)
V_{max}	maximum velocity at center (m/s)
V_s	slip velocity (m/s)
$V_z(0)$	centerline axial solids velocity, by curve fitting
$V_z(r)$	time averaged axial solid velocity (m/s)
W	blade width (m)
X	solid loading

Greek letters

α_1, α_2	empirical constants in Eq. (29)
β	inter-phase drag coefficient (kg/m^3 s)
γ	kinematic viscosity (m^2/s)
ε	turbulence eddy dissipation
$\varepsilon(r)$	time averaged radial solid holdup profile
$\varepsilon_l, \varepsilon_s$	liquid volume fraction and solid fraction
ε_{mf}	voidage at minimum fluidisation
$\bar{\varepsilon}_s$	time averaged solid holdup
ε_{sm}	maximum solid packing parameter
η	efficiency of energy transfer from liquid phase to solid phase
λ	friction factor
λ_s	friction factor for very rough pipe
μ_{leff}	total phase viscosity (kg/m s^2)
μ_{tl}	phase turbulence viscosity (kg/m s^2)
μ_{tp}	particle induced turbulence (kg/m s^2)
μ_λ	phase viscosity (kg/m s^2)
ξ	relative pipe roughness
ρ_s	density of solid phase (kg/m^3)
ρ, ρ_l	liquid density (kg/m^3)
$\Delta\rho$	density difference between liquid and solid (kg/m^3)
τ_l	liquid-phase viscous stress tensor (kg/m s^2)

Subscripts and superscripts

l	liquid phase
max	maximum
mf	minimum fluidisation
s	solid phase
α	phase
2D	two dimensional
3D	three dimension

apparent drag force, the effective gravitational force and the voidage to propose a generalised correlation applicable for laminar, intermediate and turbulent regimes. Recently, Limtrakul et al. [3] have reported a comprehensive experimental study employing non-invasive gamma ray based techniques, computer tomography and computer-aided radioactive particle tracking techniques to measure solid holdup and solid velocity profiles under different operating parameters. They reported that the average values of solids holdup in the column were in agreement with the modified Richardson–Zaki equation [10].

From a modeling perspective, Roy and Dudukovic [11] investigated liquid–solid fluid dynamics in a circulating fluidised bed riser using non-invasive flow methods and discussed the solid flow structure in the riser. They developed a CFD model for the riser and validated the findings with experimental data. Cheng and Zhu [12] developed a CFD model for liquid–solid circulating fluidised bed reactor and included turbulence and kinetic theory of granular flow in the governing equations to model the high Reynolds number two phase flows with strong particle–particle interactions. They found enhanced non-uniformities in flow structure for the larger particle system. Doroodchi et al. [13] used CFD to investigate the influence of inclined plates on the expansion behavior of solids in a liquid fluidised bed containing two different sized particles. The authors were able to validate their computational model with experiments performed with ballotini particles demonstrating a significant increase in particle sedimentation rate due to introduction of inclined plates into the conventional fluidised bed. The authors modeled the drag between the particles and continuous fluid based on experimentally determined Richardson–Zaki exponents for the various particle sizes. However, comparatively less information is available regarding CFD modeling of the solids flow pattern in a liquid–solid fluidised beds in contrast to the extensive knowledge of gas–solid fluidised beds and bubble column reactors.

The present work aims to predict the flow pattern of solids and liquid motion in liquid fluidised beds for various design and operating conditions using CFD. The data of Limtrakul et al. [3] is chosen for the purpose of validating the numerical results obtained through CFD. The non-invasive measurement techniques such as computer tomography (CT), computer-aided radioactive particle tracking (CARPT) are used for the prediction of phase holdup and solid velocity profiles respectively of liquid–solid fluids beds by Limtrakul et al. [3]. The liquid fluidised beds used in the experimental study of Limtrakul et al. [3] are two plexiglas columns: 0.1 m i.d. with 2 m height and 0.14 m i.d. with 1.5 m height. The liquid phase is chosen as water. The solid phase is chosen as glass beads of size 1 and 3 mm with a density of 2900 and 2500 kg/m^3, respectively. They also used acetate beads of 3 mm size with a density of 1300 kg/m^3.

The present work also aims to evaluate the influence of interphase drag force models, inlet boundary condition, grid resolution, time step sensitivity as well as a comparison between 2D and 3D simulation on the predictive capabilities of the numerical investigation. Based on the flow pattern of solids motion predicted by CFD, a solid circulation in the core and annular regions of the fluidised bed as well as the dissipation of energy by various phenomenon such as friction, liquid phase turbulence and mean flow have been computed. The results confirm the conservation of mass rates between core and annular regions. Energy required for solid expansion in a liquid fluidised bed has been compared with the energy required for solid suspension in equivalent stirred tank reactor.

2. Governing equations

The simulation of liquid fluidised bed was performed by solving the governing equations of mass and momentum conservation using ANSYS CFX-5 software. A multifluid Eulerian model, which considers the conservation of mass and momentum of fluid and solid phases, was applied.

- Continuity equations:

liquid phase : $\quad \dfrac{\partial}{\partial t}(\varepsilon_l \rho_l) + \nabla(\rho_l \varepsilon_l \vec{u}_l) = 0$ (1)

solid phase : $\quad \dfrac{\partial}{\partial t}(\varepsilon_s \rho_s) + \nabla(\rho_s \varepsilon_s \vec{u}_s) = 0$ (2)

where ε_l, ε_s are the volume fractions of liquid and solid phase which satisfies the relation:

$$\varepsilon_s + \varepsilon_l = 1 \tag{3}$$

u_l, u_s are the liquid and solid phase velocities and ρ_l, ρ_s are the liquid and solid phase densities, respectively.
- Momentum equations:

liquid phase :

$$\frac{\partial}{\partial t}(\rho_l \varepsilon_l \vec{u}_l) + \nabla(\rho_l \varepsilon \vec{u}_l^2) = -\varepsilon_l \nabla P + \nabla \overline{\overline{\tau}}_l + \rho_l \varepsilon_l g - F_{Dl} \tag{4}$$

solid phase :

$$\frac{\partial}{\partial t}(\rho_s \varepsilon_s \vec{u}_s) + \nabla(\rho_s \varepsilon_s \vec{u}_s^2) = -\varepsilon_s \nabla P - \nabla p_s + \rho_s \varepsilon_s g + F_{Ds} \tag{5}$$

where P is the pressure, ∇p_s the collisional solids stress tensor that represent the additional stresses in solid phase due to particle collisions, g the gravity vector, and τ_l represents the stress tensor associated with liquid phases and the last term (F_D) represents interphase drag force between liquid and solid phases.

The most popular constitutive equation for solids pressure are due to Gidaspow [14], viz.:

$$\nabla p_s = G(\varepsilon_s)\nabla \varepsilon_s \tag{6}$$

where $G(\varepsilon_s)$ is the elasticity modulus and it is given as

$$G(\varepsilon_s) = G_0 \exp(c(\varepsilon_s - \varepsilon_{sm})) \tag{7}$$

as proposed Bouillard et al. [15] where G_0 is the reference elasticity modulus and is set to 1 Pa, c the compaction modulus which is set to 100 for the present simulation and ε_{sm} is the maximum packing parameter.

Table 1
Standard values of the parameters used in the turbulence model

C_μ	0.09
σ_k	1.0
σ_ε	1.3
$C_{\varepsilon1}$	1.44
$C_{\varepsilon2}$	1.92
$C_{\mu b}$	0.6

Viscous stress term τ_l for liquid phase is given by the following equation:

$$\bar{\bar{\tau}}_l = \varepsilon_l \mu_{\text{eff},l}(\nabla \vec{u}_l + \nabla \vec{u}_l) + \varepsilon_l \left(\lambda_l - \frac{2}{3} u_l \right) \nabla u_l \bar{\bar{I}} \tag{8}$$

where μ_{eff} is the effective viscosity accounting for turbulence and is given as

$$\mu_{\text{eff},l} = \mu_l + \mu_{tl} + \mu_{tp} \tag{9}$$

where μ_l is the liquid viscosity, μ_{tl} is the liquid phase turbulence viscosity or shear induced eddy viscosity, which is calculated based on the k–ε model as

$$\mu_{tl} = c_\mu \rho_l \frac{k^2}{\varepsilon} \tag{10}$$

where the values of k and ε come directly from the differential transport equations for the turbulence kinetic energy and turbulence dissipation rate.

μ_{tp} represents the particle induced turbulence and is given by the equation proposed by Sato et al. [16] as

$$\mu_{tp} = c_{\mu b} \rho_s \varepsilon_s d_p |\vec{u}_s - \vec{u}_l| \tag{11}$$

The values used for constants in the turbulence equations are summarized in Table 1.

The interphase drag force, which is generally, computed from the knowledge of the drag coefficient C_d, particle Reynolds number, and solids volume fraction is given by

$$F_{Ds} = -F_{Dl} = C_d \frac{3}{4} \rho_l \frac{\varepsilon_s}{d_p} |\vec{u}_s - \vec{u}_l|(\vec{u}_s - \vec{u}_l) = \beta(u_s - u_l) \tag{12}$$

where β is the interphase drag coefficient.

The following drag models were used for representing the drag coefficient between solid and liquid phases.

- Drag model 1 [14]:

$$\beta = \frac{150\varepsilon_s^2 \mu_l}{\varepsilon_l d_p^2} + \frac{1.75\varepsilon_s \rho_l(u_s - u_l)}{d_p} \quad (\varepsilon_l < 0.8)\,[17] \tag{13}$$

$$\beta = \frac{3}{4} C_d \rho_l \frac{\varepsilon_s}{d_p}(\vec{u}_s - \vec{u}_l) f(\varepsilon_l) \quad (\varepsilon_l < 0.8)\,[18] \tag{14}$$

where

$$C_d = \frac{24}{Re}(1 + 0.15\,Re_p^{0.687}), \quad Re \leq 1000 \tag{15}$$

$$C_d = 0.44, \quad Re \geq 1000 \tag{16}$$

and

$$f(\varepsilon_l) = \varepsilon_l^{-1.65} \tag{17}$$

- Drag model 2 [19]:

$$\beta = \frac{3}{4} C_d \rho_l \frac{\varepsilon_s}{d_p}(\vec{u}_s - \vec{u}_l) f(\varepsilon_l) \tag{18}$$

where

$$f(\varepsilon_l) = \varepsilon_l^{-x} \tag{19}$$

where x is given as

$$x = 3.7 - 0.65 \exp\left[-\frac{1}{2}(1.5 - \log_{10} Re_p)^2 \right] \tag{20}$$

- Drag model 3 [20]:

$$\beta = \frac{3}{4} \frac{C_d}{f^2} \frac{\rho_l |u_s - u_l|}{d_p} \varepsilon_l \varepsilon_s \tag{21}$$

$$C_d = \left(0.63 + 4.8 \sqrt{\frac{f}{Re_t}} \right)^2 \tag{22}$$

where f is the ratio of the falling velocity of a superficial to the terminal velocity of a single particle and is given by [21]:

$$f = 0.5(A - 0.06Re \\ + \sqrt{(0.06Re)^2 + 0.12Re(2B - A) + A^2}) \tag{23}$$

where

$$A = \varepsilon_l^{4.14} \tag{24}$$

$$B = \begin{cases} \varepsilon_l^{2.65}, & \varepsilon_s < 0.15, \\ 0.8\varepsilon_l^{1.28}, & \varepsilon_s \geq 0.15. \end{cases} \tag{25}$$

3. Numerical simulation

ANSYS CFX-5 software code was used for simulating the hydrodynamics of liquid–solid fluidised bed. Tables 2 and 3 summarizes the model parameters/conditions used for the simulation of solid motion in liquid fluidised beds.

Table 2
Simulation process conditions

Description	Value
2D and 3D simulation	Column diameter 0.14 m, height 1.5 m
Grid size	Coarse mesh with 25,000 nodes, finer mesh with 40,000 nodes
Time step	0.001–0.01 s
Inlet boundary	Fully developed velocity profile, Uniform inlet velocity
Column diameter	Diameter: 0.1 m, 0.14 m
Particle size	1, 3 mm
Particle density	1300–2500 kg/m³
Superficial liquid velocity	0.07–0.13 m/s

Table 3
Simulation model parameters

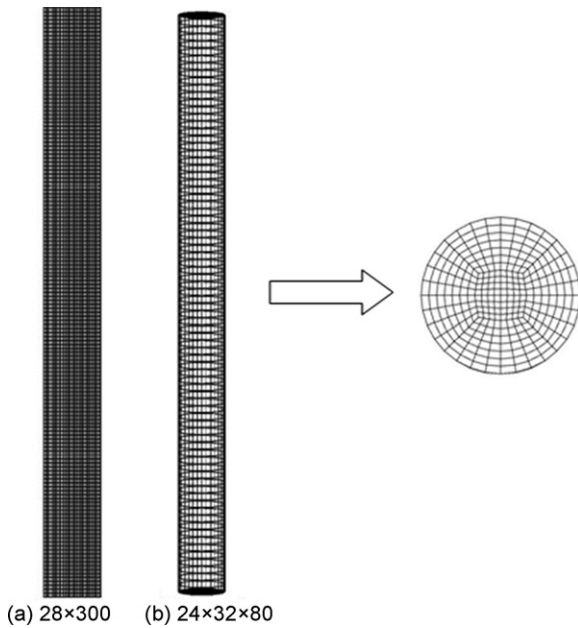| Solid	Glass beads	
Density (kg/m^3)	2500	
Size (mm)	3	1
U_{mf} (m/s)	0.0412	0.014
Solid holdup	0.683	0.593
Bed voidage	0.317	0.417
Initial bed height (m)	0.369	0.366

(a) 28×300   (b) 24×32×80

Fig. 1. (a) 2D; (b) 3D mesh of liquid fluidised bed.

3.1. Flow geometry and boundary conditions

Fig. 1 depicts typical numerical mesh used for simulation and Table 3 shows a schematic view of the initial conditions specified for the simulation. The upper section of the simulated geometry, or freeboard, was considered to be occupied by liquid only. Inlet boundary conditions were employed at the bottom of the bed to specify a uniform liquid inlet velocity. The liquid is introduced at all the computational cells of the bottom of the column. Pressure boundary conditions were employed at the top of the freeboard. This implies outlet boundary conditions on pressure, which were set at a reference value of 1.013×10^5 Pa. The lateral walls were modeled using the no-slip velocity boundary conditions for the liquid phase and the free slip assumption for the solid phase.

The numerical simulations of the discrete governing equations were achieved by finite volume method. Pressure velocity coupling was achieved by the SIMPLE algorithm. The governing equations were solved using the advanced coupled multi-grid solver technology of CFX-5. The second order equivalent to high-resolution discretization scheme of momentum, volume fraction of phases, turbulent kinetic theory and turbulence dissipation rate was chosen. During the simulations, the standard values of under relaxation factors were used. For time dependent solution the second order implicit time discretization was used. The simulations were carried out till the system reached the pseudo steady state. Once the fully developed quasi-steady state is reached, the time averaged quantities are calculated. For all the simulations, the time averaged quantities are performed in the time interval 50–150 s. The axial and azimuthally average is then performed along the axial direction within the middle section of the column. The convergence criteria for all the numerical simulation is based on monitoring the mass flow residual and the value of 1.0e−04 is set as converged value. This convergence is monitored as a function of number of iterations at each time.

Time dependent simulations were performed with time step in the range of 0.01–0.001 s. The various time steps, viz., 0.01, 0.005 and 0.001 s were used for testing the convergence and based on the convergence and computational time a value of 0.005 s was set as time step for the simulation studies in this work. Also the simulation was carried out for the liquid–solid fluidised bed geometry with 25,000 and 40,000 nodes. Based on
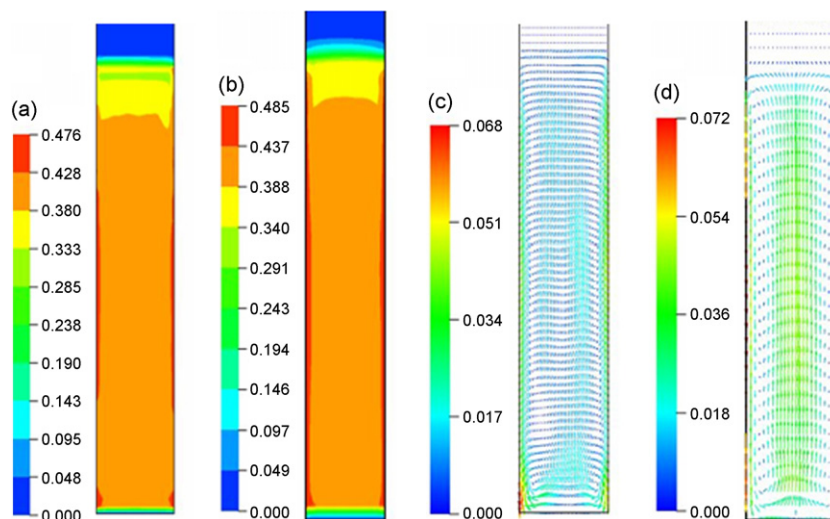

Fig. 2. Comparison of 2D and 3D simulation, time averaged solid holdup from (a) 2D; (b) 3D simulation, time averaged solid velocity from (c) 2D simulation; (d) 3D simulation.

Table 4
Comparison of bed expansion and solid holdup prediction from different drag force models and experimental data

Drag force model	Bed expansion			Solid holdup		
	Experimental	CFD	Error (%)	Experiment	CFD	Error (%)
Gidaspow [14]	0.586	0.59	+0.7	0.43	0.43	−0.7
Di Felice [19]		0.68	+16.0		0.36	−15.8
Syamlal and O'Briens [20]		0.58	−1.0		0.43	0.23

Table 5
Comparison of bed expansion and solid holdup on the type of velocity profiles at the inlet

Type of feed inlet conditions	Bed expansion			Solid holdup		
	Experimental	CFD	Error (%)	Experimental	CFD	Error (%)
Fully developed velocity profile	0.586	0.5	+14.7	0.43	0.498	−15.8
Uniform velocity profile		0.59	−0.68		0.427	+0.7

the comparison between experimental and simulated results for time averaged axial solid velocity, the mesh with 25,000 nodes is chosen for further simulation studies.

4. Results and discussion

4.1. Comparison between 2D and 3D simulation

Fig. 2 provides a comparison of time averaged solid holdup and solid velocity obtained through 2D and 3D CFD simulation. From Fig. 2(c) and (d) it is evident that 3D CFD simulation provides a more accurate prediction of solid motion involving the core-annulus pattern and hence only 3D simulation was chosen for further studies in this work.

4.2. Effect of drag force models

Fig. 3 shows the effect of drag force models proposed by Gidaspow [14], Di Felice [19] and Syamlal and O'Brien [20] by comparing the variation of axial solid velocity against dimensionless radius position. Table 4 depicts the influence of drag force models by comparing the bed expansion and solid holdup with experimental data reported by Limtrakul et al. [3]. Even though the models proposed by Syamlal and Gidaspow match closely with the experimental data of Limtrakul (average error of
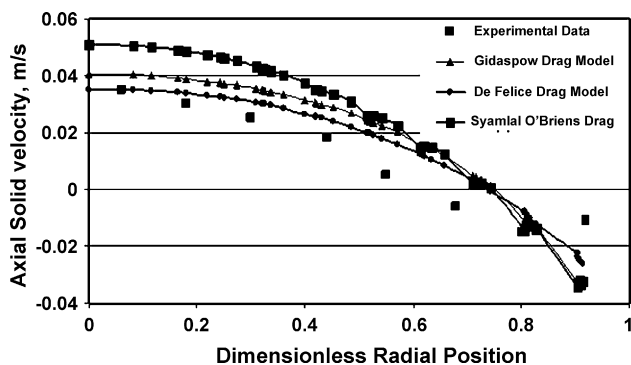

Fig. 3. Influence of different drag force models on the time averaged axial solid velocity of fluidised at a superficial liquid velocity of 0.07 m/s.

0.2–0.7% for solid holdup), the drag model proposed by Syamlal over predicts the axial solid velocity profiles. Based on these observations the Gidaspow drag model was used in the present study.

4.3. Effect of inlet feed condition

The effect of two types of inlet velocity profiles ($V_{in} = V_{max}$ $(1 − r/R)^{1/7}$, uniform velocity profile) of liquid feed was evaluated with the experimental results in the present study. Table 5 presents the effect of different inlet conditions on bed expansion and solid holdup. The fully developed inlet profile gives lower bed expansion and higher solid holdup than the velocity profiles assuming uniform velocity as shown in Table 5.

Based on the above observations, Table 6 gives the CFD model parameter used in the numerical investigation.

4.4. Comparison of solid holdup between experimental and CFD results

Fig. 4 shows the time averaged solid holdup as a function of dimensionless radial position along with the experimental results reported by Limtrakul et al. [3]. The solid holdup is defined as the volume fraction of the solid phase in the liquid–solid mixture. The solid holdup profile predicted by CFD matches closely with experimental data at the center of the column and varies at the wall region of the column with an average error of 2.6%. The enhanced deviation at the wall may be due to wall effects which have not been explicitly considered in the present study. Table 7 shows the averaged solid holdup obtained by experimental and

Table 6
Parameters employed in CFD simulation

Description	Method used
Mode of simulation	3D
Grid size	25,000 nodes
Time step	0.005 s
Drag model	Gidaspow model
Inlet boundary	Uniform inlet velocity

Table 7
Experimental validation of average solid holdup predicted by CFD

Column size (m)	Superficial liquid velocity (m/s)	Solid particle	Holdup from experimental data	Holdup from the present CFD simulation	Error (%)
0.14	0.07	Glass beads (3 mm)	0.44	0.42	+4.5
		Glass beads (1 mm)	0.51	0.48	+5.9
	0.1	Glass beads (3 mm)	0.35	0.3	+14.3
	0.13	Glass beads (3 mm)	0.25	0.255	−2.0
0.1	0.065	Glass beads (3 mm)	0.48	0.43	+10.4

CFD simulation at various operating conditions. It is observed that the solid holdup obtained from CFD simulation is able to predict the experimental results reported by Limtrakul with an average error of 2–14%.

4.5. Solid motion in liquid fluidised bed

Experimental studies of solid motion reported by Limtrakul shows that multiple solids cell circulations patterns exist for all conditions of liquid fluidised bed operations. However, CFD simulation exhibits only a single solid circulation cell which is also in agreement with the observations of Roy et al. [22] in a liquid–solid riser. Fig. 5 shows the vector plot of time averaged solid velocity on the different planes at typical operating conditions ($U_l = 0.07$ m/s) for glass beads. The existence of a single recirculation cell with solids ascending along the column at the center and descending along the wall is evident from the simulation results. CFD simulation of axial solid velocity at various dimensionless radial positions is depicted in Fig. 6. The agreement between the experimental and simulation results is quite satisfactory.

4.6. Effect of particle size and density

Acetate beads ($\rho_s = 1300$ kg/m^3) and glass beads ($\rho_s = 2500$ kg/m^3) with particle sizes, 0.001 and 0.003 m were used to study the effect of particle size and density. Fig. 7 shows that the axial solid velocities increase with increase in particle diameter and density leading to larger inversion point (the point at which zero axial solid velocity) for both CFD simulation and the experimental results reported by Limtrakul. Table 8 depicts comparison of the inversion points for different
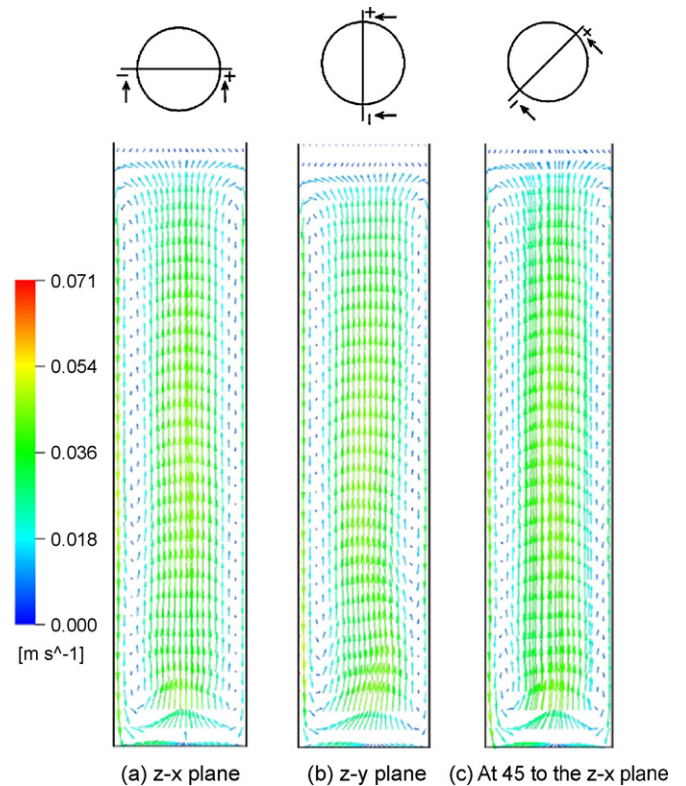
Fig. 5. Typical time averaged azimuthally averaged axial solid velocity profile: (a) z–x plane; (b) z–y plane; (c) At 45 to the z–x plane.

operating conditions. The smaller sized particle of 1mm glass beads has a smaller value of inversion point compared to that of glass beads of 3 mm size. Song and Fan [23] mentioned that due to higher value of apparent viscosity of slurry, the inversion
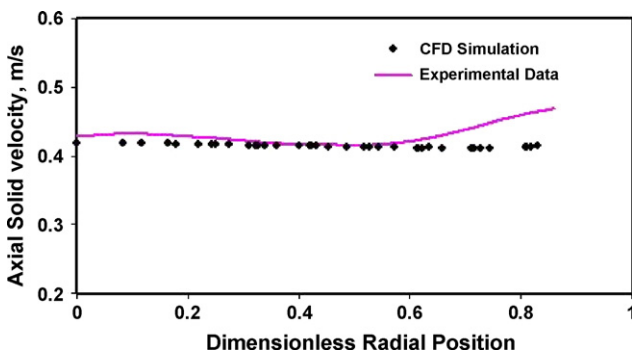
Fig. 4. Azimuthally averaged solid holdup profile obtained by CT scan and CFD simulation, 0.14 m diameter column, 0.003 m glass beads $U_l = 0.07$ m/s.
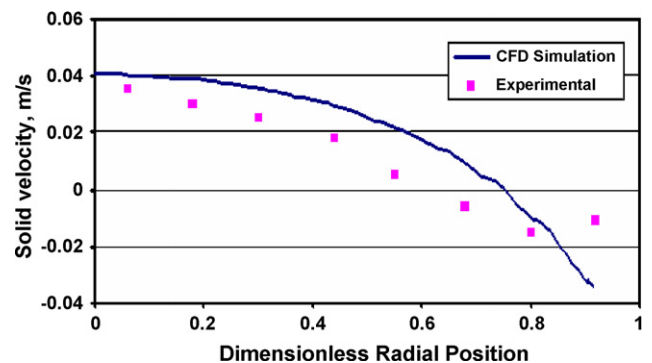
Fig. 6. Axial solid velocity profiles as a function of radial position at a superficial velocity of 0.07 m/s.

Table 8
Comparison of inversion points for different operating condition

Column diameter	Solid properties	Inversion points	
		Experimental	CFD simulation
0.14 m	Glass beads (2500 kg/m^3, 3 mm)	0.72	0.77
	Glass beads (2900 kg/m^3, 1 mm)	0.62	0.69
	Acetate beads (1300 kg/m^3, 3 mm)	–	0.64
0.1 m	Glass beads (2500 kg/m^3, 3 mm)	–	0.72

point is reduced for systems with particles having smaller sizes.

4.7. Effect of liquid superficial velocity

The increase in superficial liquid velocity increases the energy input to the system, leading to enhanced bed expansion and solid motion. Fig. 8 shows the effect of liquid superficial velocity on the time averaged axial solid velocity. The CFD predictions of axial solid velocity give the same pattern as those obtained from experimental data.

4.8. Turbulence parameters

To further validate the CFD simulation results, a comparison of the turbulence parameters, viz., turbulence intensities, and shear stress profiles with the experimental data provided by Limtrakul et al. [3] was made. Fig. 9 shows the root-mean-
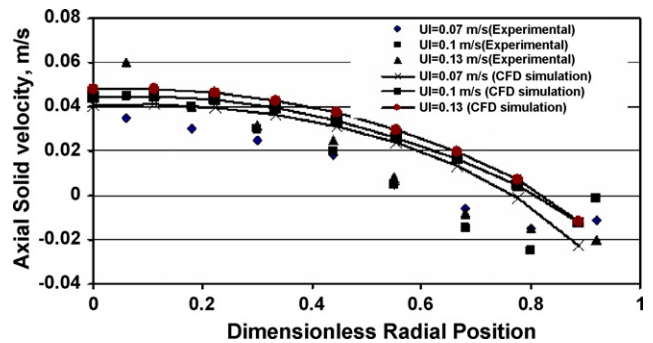

Fig. 8. Effect of superficial liquid velocity on time averaged axial solid velocity.

square (rms) axial (u'_r) and radial (u'_r) velocities of solids along the radial position. Fig. 9a and b shows that the axial rms velocities are roughly twice those of the corresponding radial components. Similar to observations made by Devanathan et al. [24] in gas–liquid bubble columns systems and Roy et al. [22] in liquid–solid riser. A typical comparison of experimental and simulation results is depicted in Figs. 9 and 10.
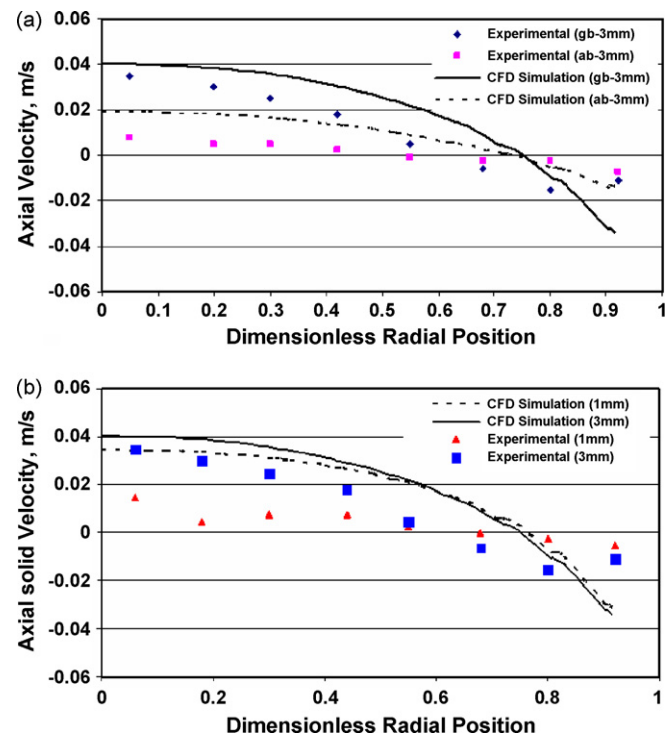

Fig. 7. (a) Effect of particle type (U_1 for glass beads = 0.007 m/s, U_1 for acetate = 0.024 m/s) and (b) effect of particle size (U_1 for 3 mm = 0.007 m/s, U_1 for 1 mm = 0.024 m/s) on axial solid velocity.
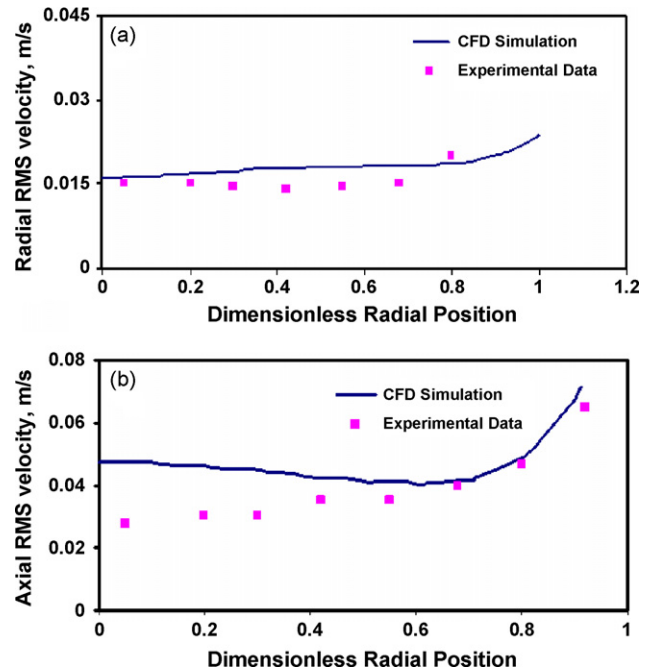

Fig. 9. (a) Variation of radial rms velocities along the radial position; (b) variation of axial rms velocities along the radial position.
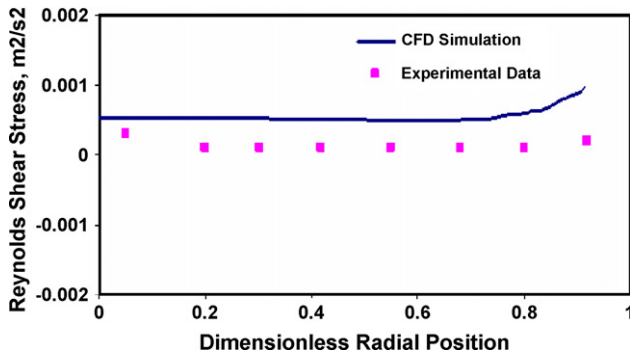
Fig. 10. Variation of Reynolds shear stress along the radial position.

5. Computation of solid circulation in the core and annular regions

Based on the validation of CFD model predictions discussed earlier, a mass balance of solids in the core and annular region was computed to verify conservation of solid mass in the liquid–solid fluidised bed, i.e. the net solid volume flow rate in core region should equal the net solid volume flow rate in the annular region represented mathematically as

$$\text{solid upflow rate in the core region} = 2\pi \int_0^{R_i} r\varepsilon(r)V_z(r)\,\mathrm{d}r \tag{26}$$

solid downflow rate in the annular region

$$= 2\pi \int_{R_i}^{R} r\varepsilon(r)V_z(r)\,\mathrm{d}r \tag{27}$$

where $\varepsilon(r)$ is the time averaged radial solid holdup profile and $V_z(r)$ is the time averaged axial solid velocity and R_i is the radius of inversion, defined as the point at which the axial solids velocity is zero. The radial solid holdup profile at each of the operating conditions proposed by Roy et al. [22] is given by

$$\varepsilon_s(r) = \bar{\varepsilon}_s \frac{m+2}{m+2+2C}\left[1+C\left(\frac{r}{R}\right)^m\right] \tag{28}$$

Similarly an expression that has been observed to describe the radial profile of the axial solids velocity [22] is

$$V_z(r) = V_z(0) + \alpha_1\left(\frac{r}{R}\right)^{n_c} - \alpha_2\left(\frac{r}{R}\right)^{n\alpha_1/\alpha_2} \tag{29}$$

In Eq. (29), $V_z(0)$ is the centerline axial solids velocity and α_1 and α_2 are empirical constants determined through curve

fitting. The exponent n_c defines the curvature of the velocity profile.

The net volumetric solid flow rates computed from Eqs. (26) and (27) are shown in Table 9. The relative deviation of volumetric solid flow between core and wall region is observed in the range of 10–15%. This finding may be compared with observation of Kiared et al. [2] who investigated the net solid flow rate in the core and annular region and obtained the relative deviation for volumetric mass rate in the range of 23–27%.

6. Computation of energy dissipation due to solid and liquid motion

The energy flows due to various contributing mechanisms in the liquid–solid fluidised bed was computed with a view to determine their relative contributions and the energy efficiency of the liquid–solid fluidisation process.

Efficiency of energy transfer to the solid phase from liquid phase may be defined as

$$\eta = \frac{\text{energy gained by solids in the reactor}\,(E_T)}{\text{energy dissipation by the liquid phase in the reactor}\,(E_D)} \tag{30}$$

The energy efficiency of the process is computed with the following assumptions based on the CFD results:

(1) solids move downwards in the annular region;
(2) liquid phase in the annular region is considered to be under pseudo-stationary state, i.e. as a stagnant fluid;
(3) the motion of solids upwards from the bottom of the liquid–solid fluidised bed to the expanded bed height is due to increase in its potential and kinetic energy;
(4) the solid phase kinetic energy is computed from the relative motion between the solid phase and liquid phase;
(5) the interface between the core and annular region is assumed equivalent to as a rough wall containing solid particles for computing friction loss of the liquid phase.

6.1. Energy transfer to solid phase from the liquid phase (E_T)

The total energy of solids in the core region is computed as the sum of potential energy (E_s) and solid phase kinetic energy (E_B). Thus:

$$E_T = E_s + E_B \tag{31}$$

Table 9
Mass balance of solid circulation flow in liquid fluidised bed

Column size (m)	Liquid superficial liquid velocity (m/s)	Solid particle	Volumetric flow rate of solid in core (m³/s)	Volumetric flow rate of solid in annulus (m³/s)	Relative deviations (%)
0.14	0.07	Glass beads (3 mm)	1.614E−05	1.86E−05	13.1
	0.07	Glass beads (1 mm)	1.236E−05	1.506E−05	17.9
	0.1	Glass beads (3 mm)	8.303E−06	8.563E−06	3.0
	0.13	Glass beads (3 mm)	6.3507E−06	5.629E−06	12.8
	0.024	Acetate beads (3 mm)	5.3572E−06	5.339E−06	0.03

The solid phase potential energy is given by

$$E_s = \rho_s g H \frac{\pi}{4} D_c^2 v_s \tag{32}$$

where v_s is the time averaged solid velocity in the core region and D_c is the diameter of the core region.

The solid phase kinetic energy is the energy gained by solids through relative motion between liquid phase and solid particles represented by the interfacial frictional force. The rate of energy transfer by friction between the two phases is calculated based on the drag force and slip velocity which is summed over all the particles. For a single particle at an infinite expanded state ($\varepsilon = 1$), the interaction can be represented as the sum of drag and buoyancy forces, thus:

$$mg = \text{drag} + \text{buoyancy},$$

$$\frac{\pi}{6} d_p^3 (\rho_s - \rho_l) = C_d \frac{\pi}{4} d_p^2 (U_l - U_s)|U_l - U_s| \frac{\rho_l}{2} \tag{33}$$

For multiple particles, the above equation can be written as

$$\frac{\pi}{6} d_p^3 (\rho_s - \rho_l) f(\varepsilon) = C_d \frac{\pi}{4} d_p^2 (U_l - U_s)|U_l - U_s| \frac{\rho_l}{2} \tag{34}$$

Lewis and Bowerman [25], Wen and Yu [18] and Kmiec [21] presented the above equation in the form of

$$\frac{\pi}{6} d_p^3 (\rho_s - \rho_l) \varepsilon^n = C_d \frac{\pi}{4} d_p^2 (U_l - U_s)|U_l - U_s| \frac{\rho_l}{2} \tag{35}$$

where $n = 4.65$ (Lewis et al.), $n = 4.7$ (Wen and Yu), and $n = 4.78$ (Kmiec).

Yang and Renken [9] developed an equilibrium force model for liquid–solid fluidised bed and derived an empirical correlation for equilibrium between forces to account for laminar, turbulent and intermediate region as given by

$$C_d \frac{\pi}{4} d_p^2 (U_l - U_s)|U_l - U_s| \frac{\rho_l}{2}$$
$$= \frac{\pi}{6} d_p^3 (\rho_s - \rho)(a\varepsilon^{4.78} + (1-a)\varepsilon^{2.78}),$$
$$a = 0.7418 + 0.9674 Ar^{-0.5},$$
$$1 < Re_t < 50, 24 < Ar < 3000,$$
$$a = 0.7880 - 0.00009 Ar^{0.625},$$
$$50 < Re_t < 500, 3000 < Ar < 10^5 \tag{36}$$

The total drag force is thus equal to the product of drag force for single particle and multiplied by the total number of particles namely:

$$F_T = \frac{\pi}{4} D^2 H \varepsilon_s g (\rho_s - \rho_l)(a\varepsilon^{4.78} + (1-a)\varepsilon^{2.78}) \tag{37}$$

The rate of energy transferred to the solid from liquid motion is computed from Eqs. (36) and (37) as

$$E_B = \frac{\pi}{4} D^2 H \varepsilon_s g (\rho_s - \rho_l)(a\varepsilon^{4.78} + (1-a)\varepsilon^{2.78}) V_s \tag{38}$$

where V_s is the slip velocity.

6.2. Energy dissipation by the liquid phase (E_D)

energy dissipation by the liquid phase (E_D)

= input energy due to liquid flow into the fluidised bed (E_i)

　−[energy dissipation due to liquid phase turbulence (E_e)

　+potential energy of liquid leaving from the fluidised bed (E_l)

　+kinetic energy of liquid leaving from the fluidised bed (E_k)

　+frictional energy loss at the interface between

　　coreandannularregion (E_f)] $\tag{39}$

6.2.1. Input energy due to liquid flow

The input energy due to liquid flow is computed as

$$E_i = \frac{\pi}{4} D^2 H g V_l (\varepsilon_s \rho_s + \varepsilon_l \rho_l) \tag{40}$$

where D is the diameter of the column, H the expanded bed height, V_l the superficial liquid velocity and ε_l, ε_s are the volume fraction of liquid phase and solid phase, respectively.

6.2.2. Liquid phase turbulent energy dissipation (E_e)

k–ε model is used for the prediction of flow pattern, to obtain the radial and axial variation of ε (energy dissipation rate per unit mass). The total energy dissipation in liquid phase is calculated through volume integration of ε in the axial and radial directions.

6.2.3. Potential energy of liquid leaving the fluidised bed (E_l)

The liquid leaving the bed possesses potential energy by virtue of its expanded bed height given by

$$E_l = \frac{\pi}{4} D^2 H g V_l \rho_l \tag{41}$$

6.2.4. Kinetic energy of liquid leaving the fluidised bed (E_k)

The liquid leaving the bed possesses the kinetic energy by virtue of its velocity given by

$$E_k = \frac{1}{2} \rho_l \frac{\pi}{4} D^2 V_l^3 \tag{42}$$

6.2.5. Energy loss at the interface between the core and annular region (E_f)

Since the flow patterns of liquid–solid fluidised bed represented as core and annular regions, energy losses due to friction will occur at the interface between the core and annular region.

Sarimeseli [26] developed a correlation to compute the friction factor for sedimenting particles in rough pipes represented by the following expression, viz.:

$$\lambda = \lambda_s + (0.79 \ln Re - 1.64 + (\xi Re)^{1/2})^{-2} \quad (Re > 3000) \tag{43}$$

where λ is the friction factor.

λ_s is the friction factor for very rough pipes and is defined as

$$\frac{1}{\lambda_s} = -4 \log \left(\frac{\xi}{3.7} \right) \tag{44}$$

ξ is the relative pipe roughness defined as ε/D and ε is the height of roughness factor which is equal to size of the particle and D is the diameter of pipe.

Thus, frictional energy loss of liquid phase at the interface can be calculated as

$$E_f = \frac{\lambda^* \langle V \rangle^2}{2} \tag{45}$$

Based on the above assumptions, friction energy loss at the interface between core and annular region was computed and the values are in the range 1e−04 to 1e−05 W.

Table 10 illustrates the magnitude of various components of energy dissipation. Based on a range of particle size and density, liquid superficial velocity and column dimension, it is observed the overall efficiency of energy for solid fluidisation in a liquid medium is in the range of 80–90%.

It is of interest to compare the energy dissipation in liquid–solid fluidised bed with an equivalent stirred reactor. The comparison is based on the equivalence of solid suspension cloud height with expanded height of solid in liquid–solid fluidised bed. Joshi and coworkers [27] developed the critical impeller speed for just suspended solids in the stirred reactor and concluded that pitched blade downward pumping to be most energy efficient for the suspension of solid particles and has developed following correlation for critical impeller speed and given as

$$N_{CS} = \frac{f_c \gamma^{0.1} (g \Delta\rho/\rho_l)^{0.45} X^{0.1} d_p^{0.11} T^{0.31}}{D_i^{1.16}}, \quad \text{for } 100 < d_p$$

$$< 2000\,\mu m, \ 0 < X < 50\,\text{wt.\%}, \ 0.175$$

$$< D_i/T < 0.58 W/D_i = 0.3 \tag{46}$$

The following assumptions are considered to compute the power consumption for solid suspension of an equivalent stirred tank reactor theoretically:

- The volume of expanded bed of liquid fluidised bed is equivalent to volume of stirred tank reactor and height of liquid level is equal to diameter of stirred tank contactor.
- Impeller of stirred vessel is assumed as standard configuration for a 45° pitched blade turbine impeller with four blades [27].
- Power number for pitched blade turbine impeller is assumed as 1.2 in the Reynolds number range of 1.0e+05 to 1.2e+05 [28].

Operating conditions used in liquid fluidised bed includes mass of 9.7 kg solid particles (3 mm and 2500 kg/m³), superficial liquid velocity of 0.1 m/s and expanded bed height of 0.84 m (solid fraction of 0.299 and voidage of 0.701).

Thus, volume of expanded fluidised bed = 0.0129 m³ and which is considered as the volume of stirred tank reactor.

Operating conditions considered in stirred vessel contactor includes diameter of stirred tank of 0.254 m, solid mass fraction

Table 10
Efficiency of energy transfer to solid phase from liquid phase

Column size (m)	U_l (m/s)	Solid particle	E_i (Eq. (40))	E_l (Eq. (41))	E_e	E_k (Eq. (42))	E_f (Eq. (45))	E_D (Eq. (39))	E_B (Eq. (38))	E_s (Eq. (32))	$E_T = E_B + E_s$ (Eq. (37))	$\eta = E_T/E_D$ (%) (Eq. (30))
0.14	0.07	Glass beads (3 mm)	10.05	6.11	0.13	2.6 e−3	4.1e−5	3.80	0.44	2.66	3.10	81.51
	0.07	Glass beads (1 mm)	8.58	4.32	0.05	2.6e−3	6.8e−5	4.21	0.07	3.34	3.42	81.26
	0.1	Glass beads (3 mm)	18.35	12.65	0.2	7.7e−3	7.9e−5	5.50	1.18	3.76	4.94	89.94
	0.13	Glass beads (3 mm)	27.09	19.57	0.36	0.017	1.3e−4	7.16	1.95	3.73	5.68	79.54
	0.024	Acetate beads (3 mm)	1.97	1.72	4. e−4	1.1e−4	5.8e−6	0.25	0.02	0.18	0.20	80.48
0.1	0.07	Glass beads (3 mm)	10.16	6.18	0.14	1.3e−3	7.1e−5	3.83	0.48	2.52	3.0	78.26

Table 11
Comparison of power consumption in fluidised bed and stirred tank reactor

Column size (m)	U_l (m/s)	Solid particle	Power required in fluidised bed (W)	Power required in stirred tank reactor (W)
0.14	0.07	Glass beads (3 mm)	10.1	32.7
	0.07	Glass beads (1 mm)	8.6	24.5
	0.1	Glass beads (3 mm)	18.4	36.5
	0.13	Glass beads (3 mm)	27.4	38.7
	0.024	Acetate beads (3 mm)	2.0	1.8
0.1	0.07	Glass beads (3 mm)	10.2	32.7

of 0.518, impeller diameter of 0.0847 m and impeller clearance of 0.0847 m.

Thus, critical impeller speed (N_{CS}) = 15.78 r/s (computed from the Joshi correlation).

$N_{Re}(ND_i^2\rho/\mu) = 1.1 \times 10^5$, $N_p = 1.2$ and computed power consumption ($N_p\rho N^3 D_i^5$) = 36.5 W.

Table 11 illustrates the comparison of power consumption of liquid fluidised with an equivalent stirred vessel. It shows that the power consumption for stirred tank contactor is approximately three times that of fluidised bed reactor at the same operating conditions and at equivalent conditions for solid suspension. Further investigations are required to elucidate the influence of scale of operation on the relative merits between stirred contactor and liquid–solid fluidised bed for solid suspension.

7. Conclusions

CFD simulation of hydrodynamics and solid motion in liquid fluidised bed were carried out by employing the multifluid Eulerian–Eulerian approach. Adequate agreement was demonstrated between CFD simulation results and experimental findings reported by Limtrakul et al. [3] using non-invasive techniques to measure solid holdup, solid motion and turbulence parameters. The predicted flow pattern demonstrates that the time averaged solid velocity profile exhibits axisymmetric with downward velocity at the wall and maximum upward velocity at the center of the column and higher value of solid holdup at the wall and lower value of that at the center. CFD model has been further extended to compute solid mass balance in the core and annular regions and energy flows due to various contributing dissipation mechanisms. The results confirm the conservation of mass between core and annular region with a relative deviation in the range of 10–15%. The efficiency of energy transfer to the solid phase from liquid phase was computed to be in the range of 80–90%. Energy required for solid expansion in liquid fluidised bed was compared with energy required for solid suspension in an equivalent stirred tank contactor and it was found that the power consumption for stirred tank contactor is approximately three times that of fluidised bed reactor at the equivalent operating conditions.

In the present study, the influence of various interphase drag models on solid motion in liquid fluidised bed was studied. The drag models proposed by Gidaspow [14], Syamlal and O'Brien [20], and Di Felice [19] can qualitatively predict the flow pattern of solid motion inside the fluidised bed, in which the model proposed by Gidaspow gives the best agreement with experi-

mental data. To identify the CFD methodology to enhance the accuracy of numerical simulation comparison between 2D and 3D simulation, the effect of grid sensitivity, time step sensitivity and effect of inlet feed conditions were investigated and a comprehensive CFD methodology was established to model the liquid–solid fluidised bed.

References

[1] N. Epstein, Application of liquid–solid fluidisation, Int. J. Chem. Reactor Eng. 1 (2004) R1.

[2] K. Kiared, F. Larachi, M. Cassanello, J. Chaouki, Flow structure of the solids in a three-dimensional liquid fluidised bed, Ind. Eng. Chem. Res. 36 (1997) 4695–4704.

[3] S. Limtrakul, J. Chen, P.A. Ramachandran, M.P. Dudukovic, Solids motion and holdup profiles in liquid fluidised beds, Chem. Eng. Sci. 60 (2005) 1909–1920.

[4] M.P. Dudukovic, F. Larachi, P.L. Mills, Multiphase reactor—revisted, Chem. Eng. Sci. 54 (1999) 1975–1995.

[5] J. Richardson, W. Zaki, Sedimentation and fluidisation. Part I, Trans. IChemE 32 (1954) 35–52.

[6] B.A.J. Latif, J.F. Richardson, Circulation patterns and velocity distributions for particles in a liquid fluidised bed, Chem. Eng. Sci. 27 (1972) 1933–1948.

[7] L.G. Gibilaro, I. Hossain, P.U. Foscolo, Aggregate behaviour of liquid fluidised beds, Can. J. Chem. Eng. 64 (1986) 931–938.

[8] R. Di Felice, Review article on hydrodynamics of liquid fluidisation, Chem. Eng. Sci. 50 (8) (1995) 1213–1245.

[9] J. Yang, A. Renken, A generalized correlation for equilibrium of forces in liquid–solid fluidised beds, Chem. Eng. J. 92 (2003) 7–14.

[10] J. Garside, M.R. Al-Dibouni, Velocity–voidage relationship for fluidisation and sedimentation, Ind. Eng. Chem. Process Des. Dev. 16 (1977) 206–214.

[11] S. Roy, M.P. Dudukovic, Flow mapping and modeling of liquid–solid risers, Ind. Eng. Chem. Res. 40 (2001) 5440–5454.

[12] Y. Cheng, J.X. Zhu, CFD modeling and simulation of hydrodynamics in liquid–solid circulating fluidised bed, Can. J. Chem. Eng. 83 (2005) 177–185.

[13] E. Doroodchi, K.P. Galvina, D.F. Fletcherb, The influence of inclined plates on expansion behaviour of solid suspensions in a liquid fluidised bed—a computational fluid dynamics study, Powder Technol. 160 (2005) 20–26.

[14] D. Gidaspow, Multiphase Flow and Fluidisation, 1st ed., Academic Press, San Diego, 1994.

[15] J.X. Bouillard, R.W. Lyczkowski, D. Gidaspow, Porosity distribution in a fluidised bed with an immersed obstacle, AIChE J. 35 (1989) 908–922.

[16] Y. Sato, M. Sadatomi, K. Sekoguchi, Momentum and heat transfer in two-phase bubble flow, Int. J. Multiphase Flow 7 (1981) 167–177.

[17] S. Ergun, Fluid flow through packed columns, Chem. Eng. Prog. 48 (1952) 89–94.

[18] C.Y. Wen, Y.H. Yu, Mechanics of fluidisation, Chem. Eng. Prog. Symp. Ser. 62 (1966) 100–111.

[19] R. Di Felice, The voidage functions for fluid–particle interaction system, Int. J. Multiphase Flow 20 (1994) 153–159.

[20] M. Syamlal, T.J. O'Brien, Simulation of granular layer inversion in liquid fluidised beds, Int. J. Multiphase Flow 14 (1988) 473–481.

[21] A. Kmiec, Equilibrium of forces in a fluidised bed-experimental verification, J. Chem. Eng. 23 (1982) 133–136.

[22] S. Roy, A. Kemoun, M.H. Al-Dahhan, M.P. Dudukovic, Experimental investigation of the hydrodynamics in a liquid–solid riser, AIChE J. 51 (2005) 802–835.

[23] G. Song, L.S. Fan, Rheological behavior of a gas–liquid–solid fluidised bed, in: Proceedings of the World Congress III of Chemical Engineering, vol. 3, 1986, pp. 540–607.

[24] N. Devanathan, D. Moslemian, M.P. Dudukovic, Flow mapping in bubble columns using CARPT, Chem. Eng. Sci. 45 (1990) 2285–2291.

[25] E.W. Lewis, E.W. Bowerman, Fluidisation of solid particles in liquids, Chem. Eng. Prog. 48 (1952) 603–611.

[26] A. Sarimeseli, Sedimentation of particles in developed turbulent flow in rough pipes, Powder Technol. 127 (2002) 144–148.

[27] K.S.M.S. Raghava Rao, V.B. Rewatkar, J.B. Joshi, Critical impeller speed for solid suspension in mechanically agitated solid–liquid contactor, AIChE J. 34 (1988) 1332–1340.

[28] V.B. Rewatkar, K.S.M.S. Raghava Rao, J.B. Joshi, Critical impeller speed for solid suspension in mechanically agitated three phase reactors 1. Experimental part, Ind. Eng. Chem. Res. 30 (1991) 1770–1784.